Membrane-Based Absorption of VOCs from a Gas Stream

Tarun K. Poddar, Sudipto Majumdar, and Kamalesh K. Sirkar
Dept. of Chemical Engineering, Chemistry and Environmental Science, New Jersey Institute of Technology, Newark, NJ 07102

A regenerative absorption-based process was developed for removing VOCs from N_2 in an inert, nonvolatile, organic liquid flowing in compact hollow-fiber devices. The process eliminates flooding, loading, and entrainment, and can replace activated carbon adsorption. Two types of hollow-fiber membranes were studied: one with a microporous wall and the other with a highly VOC-permeable nonporous coating on the outer surface of a microporous hollow fiber. Criteria for nondispersive operation were developed for each case. Experiments were conducted for the absorption of acetone, methylene chloride, toluene, and methanol from the respective VOC-N_2 gas mixture using two absorbents: silicone oil and mineral oil. The highest mass-transfer coefficient was obtained for toluene followed by methylene chloride, acetone, and methanol. Different resistances making up the overall resistance in VOC absorption were characterized comprehensively to develop a predictive capability and compare the absorption performances of two types of fibers and the two absorbents. The absorbent-filled porous membrane contributed significantly to the total mass-transfer resistance. Numerical simulations of governing equations based on a cell model agree well with experimental results.

Introduction

Air and nitrogen (purge) emissions from chemical plants/processes are contaminated by volatile organic compounds (VOCs). Common methods of reducing VOC emissions are adsorption on activated carbon, absorption, incineration/thermal oxidation, or catalytic oxidation. Each method has significant strengths as well as considerable weaknesses. Efforts are underway to develop better techniques (Armand et al., 1990; Baker et al., 1989; Mukhopadhyay and Moretti, 1993). One such technique, namely, vapor permeation, uses nonporous VOC-selective polymeric membranes (Peinemann et al., 1986). VOC-contaminated air, usually available at atmospheric pressure, flows on one side of the membrane; a vacuum is applied on the other side. The permeate is condensed to recover VOCs; the noncondensibles are returned to the feed. The partial pressure driving force for selective VOC permeation through the membrane is usually small. This driving force decreases further along the membrane device as VOC concentration drops in the treated feed. It is uneconomic to bring down the VOC concentration below 100–200 ppmv, since a large fraction of the feed air appears in the permeate; the process becomes essentially condensation of VOC from feed.

We have employed here highly efficient hollow-fiber membrane-based absorption to remove VOCs from N_2/air. Contaminated air/N_2 flows through the bores of the hollow fibers. A suitable absorbent liquid having a high solubility for the VOC is pumped countercurrently over the outside of the fibers (Figure 1). The absorbents studied here are inert, nontoxic, essentially nonvolatile organic solvents. The VOCs, effectively removed from N_2/air to the desired level, are concentrated in the absorbent, which rejects air/N_2 almost completely. They are recovered and the absorbent regenerated by applying vacuum (and/or by heating the spent absorbent) in a separate hollow-fiber membrane stripper. Such devices have many advantages: very high gas–liquid interfacial area per unit volume; independent control of gas and liquid flow rates without problems like flooding, loading, weeping, etc.; no entrainment of drops; much higher volumetric mass-transfer coefficient than conventional contactors; known gas–liquid interfacial area and modular nature. This technology has addi-

Correspondence concerning this article should be addressed to K. K. Sirkar.
T. K. Poddar is currently at the Commodore Separation Technologies, Columbus, OH 43212.

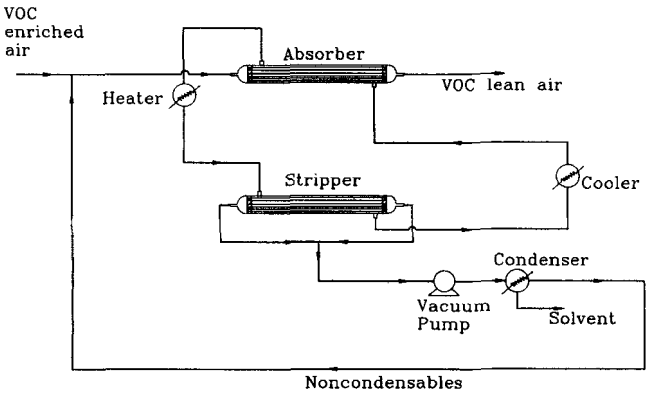

Figure 1. VOC cleanup from air by simultaneous absorption stripping.

tional advantages over the vapor permeation technology. Since N_2 has very low solubility in the absorbent, the vacuum-pump capacity will be extremely small. The absorbent oil does not absorb any moisture from feed air/N_2; this prevents ice formation in the VOC condenser after the stripper.

This article deals primarily with absorption of VOCs. A glimpse of the performance of the absorber–stripper combination is also provided here. Details of the latter along with a model have been communicated elsewhere (Poddar et al., 1995). The present technique will make VOC destruction much more efficient than direct incineration of VOCs in air; a much smaller volume of liquid is to be incinerated. Further, the recovered VOCs will act as fuel, eliminating supplemental fuel-firing.

Two novel types of membrane absorption have been studied. In the *first type*, the hydrophobic fibers are microporous, the absorbent contacting N_2/air spontaneously wets the pores, and the absorbent pressure is less than that of the gas (Figure 2a) to achieve nondispersive gas absorption. The gas–liquid contacting interface, located at the pore mouth, is on the gas side of the fiber. This is unlike hollow fiber gas–liquid contactors for aqueous absorbents where the pore is usually gas-filled, the absorbent that does not wet the hydrophobic fibers is at a pressure higher than that of the gas, and the gas–liquid interface is on the liquid side of the fiber (Zhang and Cussler, 1985; Semmens et al., 1989; Karoor and Sirkar, 1993). For VOC recovery from air in microporous membrane contactors using organic solvents wetting the membrane pores, Jansen et al. (1993) did not pursue this strategy of appropriate pressure differential conditions for successful stabilization of gas–liquid interface at the pore mouth on the gas side of the membrane.

In the *second type*, the microporous hydrophobic hollow fiber has an ultrathin but *highly VOC-permeable* plasma polymerized nonporous silicone skin on the outside surface. To achieve nondispersive absorption, the phase pressure conditions identified and demonstrated here are different (Figure 2b). Trace absorbent contamination of N_2/air is also reduced by orders of magnitude: the nonporous skin is a significant barrier to permeation of the higher molecular-weight absorbent. The absorbent may flow through the tube side or the shell side. We have studied here shell-side absorbent flow to

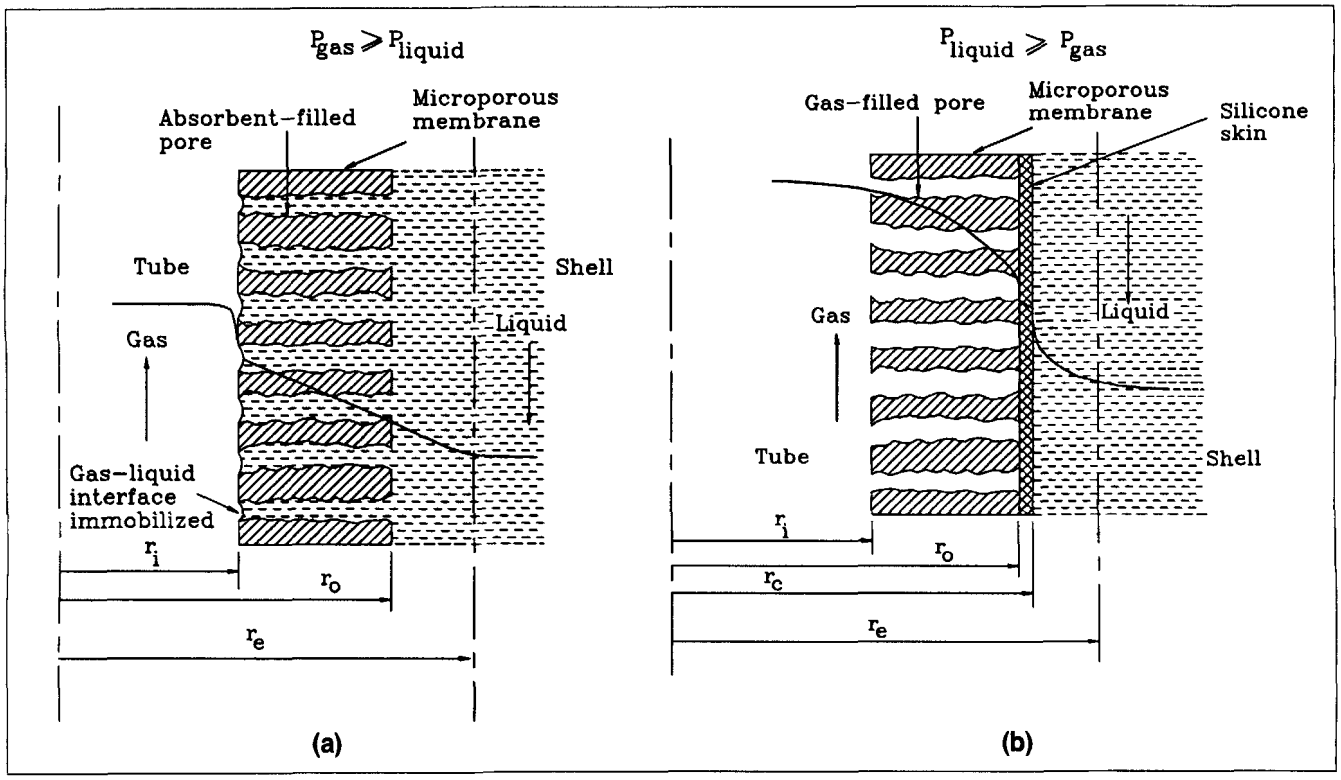

Figure 2. Local particle-pressure and concentration of VOC being absorbed.

(a) In a microporous/porous hollow-fiber module; (b) in a module having microporous/porous hollow fibers with a nonporous silicone skin on the outer surface.

Table 1. Geometrical Characteristics of Hollow Fiber Modules

Module No.	Type of Fiber	Fiber ID cm	Fiber OD cm	Eff. Length cm	Shell ID cm	No. of Fibers	Void Fraction %	Mass-Transfer Area cm^2		Mass Transfer Area per Unit Vol. cm^2/cm^3	
								+	++	+	++
1	Celgard* X-10	0.01	0.015	35.7	0.60	600	62.5	1,009	673	100.0	66.7
2	Celgard X-10	0.01	0.015	31.0	0.37	102	83.2	149	99	44.7	29.8
3	Celgard** with a silicone skin	0.024	0.030	20.5	0.80	300	57.8	580	464	56.2	45.0

*Fiber tortuosity: 2.5; surface porosity: 0.3 (Prasad and Sirkar, 1988). Hoechst Celanese SPD, Charlotte, NC.
**AMT Inc., Minnetonka, MN.
+ Based on outside diameter.
++ Based on inside diameter.

eliminate liquid-phase transfer resistance in the support pores beneath the nonporous skin. Further, pressure drop in the liquid phase would be much higher in case of tube-side absorbent flow. Figures 2b illustrates the partial pressure profile of a VOC being absorbed through such a skinned membrane.

For shell-side organic absorbent flow and tube-side gas flow, we propose that the liquid and the gas pressures should be essentially equal or the liquid pressure should be higher for the skinned membrane (Figure 2b). If the gas pressure is higher, gases such as O_2 and N_2 will permeate easily through the silicone skin and bubble through the flowing organic solvent. This may or may not be beneficial to the VOC mass-transfer process but it will certainly not be nondispersive. Further, these air or N_2 bubbles will be contaminated with VOCs and would need to be recycled to the feed gas after disengagement from the absorbent at the module end.

The skinned fibers used here are different from microporous fibers having a nonporous coating. The nonporous skin formed by plasma polymerization on the microporous hollow fiber develops an integral bonding with the substrate and has a much greater resistance to delamination and solvent swelling. A module made out of such coated fibers was also used for stripping in the simultaneous absorption-stripping process. Conventional silicone coatings develop leaks and detachment from the substrate, leading to performance instability and deterioration (Kvaerner Engineering, 1993).

Two absorbents were used: silicone oil 50 cs and Paratherm. The VOCs investigated, acetone, methanol, methylene chloride, and toluene, cover broad classes of VOCs encountered. Low feed VOC concentrations (maximum of 1,000 ppmv) were used with two types of fibers to explore absorption as a polishing technology in competition with activated carbon adsorption. This work involves development of mathematical models as well. Of the many closed-loop simultaneous absorption–stripping experiments conducted (Poddar et al., 1996), a few will be illustrated here. Different parameters, for example, diffusivity of VOCs in the absorbent liquids, permeability of different VOCs through the nonporous silicone skin of skinned fibers, and Henry's law constant for different combinations of VOCs and absorbent, are needed and were determined by independent experiments.

Experimental Studies

Hydrophobic microporous hollow fibers are Celgard X-10 of polypropylene (Hoechst Celanese, Charlotte, NC). The second type of fiber had an ultrathin ($\sim 1\mu m$) plasma polymerized layer of silicone on the outside surface of the first type of fiber (AMT, Minnetonka, MN). Table 1 provides geometrical characteristics of parallel-flow modules (fluids are in countercurrent flow) made using these two types of fibers. Detailed fabrication procedures are available in Poddar (1995). The absorbents were silicone oil 200 fluid (Dow Corning, Midland, MI) and Paratherm NF (Paratherm Corp., Conshohocken, PA). Paratherm NF oil, mineral oil based, is very stable and has an extremely low vapor pressure [0.001 mm Hg at 100°F (38°C)]. Each VOC-N_2 mixture was either obtained in a primary standard cylinder or prepared by blending the gas from such a cylinder with pure N_2.

Experimental setup and procedure for absorption

In gas absorption experiments (Figure 3), fresh absorbent from a storage vessel was pumped by a metering pump (10313M, LMI, Milton Roy, Acton, MA) through the shell side of the module. A closed cylinder partially filled with the absorbent liquid and connected to the bypass of the pump discharge line was used as a pulse dampener. The spent absorbent liquid was collected in a separate vessel. The VOC-N_2 feed-gas mixture was sent from a cylinder into the fiber bores countercurrent to the absorbent flow. Beyond the membrane module, the gas was passed through a back-pressure regulator (to maintain appropriate gas pressure in the module) into a gas chromatograph (GC) (3400 STAR, Varian, Sugarland, TX). In experiments using an absorption module made of Celgard X-10 fibers, the tube-side outlet pressure of gas was maintained at around 122 kPa (3 psig). When hollow fibers having a nonporous ultrathin skin were used for absorption, the pressures of the gas phase and the liquid phase were essentially atmospheric *unless otherwise mentioned.* All studies were done at room temperature (23 ± 1°C). Steady state was monitored by measuring the exit gas concentrations with a flame ionization detector (FID) in the Varian 3400 Star GC using a 6′ × 1/8″ column containing 0.3% Carbowax 20M on

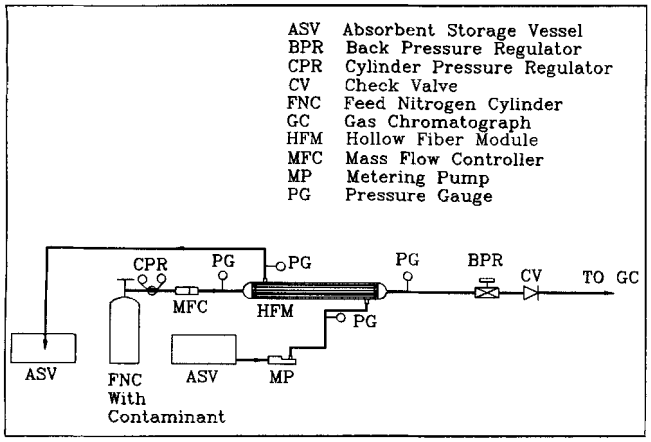

Figure 3. Experimental setup for VOC absorption.

a Carbopack C support (Varian, Sunnyvale, CA). For GC analysis, the column, injector and detector temperatures were maintained at 150, 220 and 250°C, respectively.

Simultaneous absorption-stripping experiments were conducted by running the absorption and stripping in a combined fashion (Poddar et al., 1996). Spent absorbent liquid exiting from the absorber was regenerated in the stripper (module 3) by applying full vacuum through its tube side.

The overall gas-phase-based mass-transfer coefficient, K_{oG}, for any VOC was calculated from the exit gas-phase VOC concentration data by Eq. 1:

$$K_{oG} = \frac{(pV)_{\text{ref}} * 10^{-9}}{RT * 14.7 * 60} \frac{(\text{ppmv}_{\text{in}} - \text{ppmv}_{\text{out}})}{A_m (\Delta C)_{lm}}. \quad (1)$$

Here $(\Delta C)_{lm}$ is the logarithmic mean driving force based on gas-phase concentrations:

$$(\Delta C)_{lm} = [(C_{ig,\text{in}} - C^*_{ig,\text{out}}) - (C_{ig,\text{out}} - C^*_{ig,\text{in}})]/[\ln(C_{ig,\text{in}} - C^*_{ig,\text{out}})/(C_{ig,\text{out}} - C^*_{ig,\text{in}})], \quad (2)$$

where $C^*_{ig,\text{out}}$ and $C^*_{ig,\text{in}}$ are hypothetical gas-phase concentrations in equilibrium with the absorbent concentrations at the liquid outlet and the inlet, respectively. The values of $C^*_{ig,\text{out}}$ and $C^*_{ig,\text{in}}$ are obtained from the corresponding liquid-phase VOC concentrations and the Henry's law constant H_i for the VOC:

$$C^*_{ig} = C_{il}/H_i. \quad (3)$$

Liquid-phase outlet concentration of VOC was obtained from material balance:

$$C_{il,\text{out}} = (pV)_{\text{ref}}(\text{ppmv}_{\text{in}} - \text{ppmv}_{\text{out}})\ 10^{-9}/RTV_l. \quad (4)$$

Measurement of physical parameters

The permeance of a VOC was measured by passing a VOC-N_2 gas mixture through the shell side of the module at a predetermined flow rate; its pressure was fixed by adjusting the back-pressure regulator. These values were such that an appreciable flow of gas was available at both feed outlet and permeate outlet, that is, in the shell-side and the tube-side outlets, respectively. The feed outlet and the permeate flow rates were measured by bubble flowmeters. The feed outlet VOC composition was monitored at regular intervals till steady state was achieved, typically, within 3 to 4 h.

Diffusivity of a VOC in an absorbent liquid was measured indirectly by carrying out sweep gas-driven VOC permeation from N_2 through the absorbent liquid immobilized in the pores of the porous hollow fiber. VOC-N_2 stream was passed through the tube side at a fixed rate; the pressure was maintained at 135.8 kPa (5 psig) at the exit. Pure N_2 was passed at a defined flow rate through the shell-side countercurrent with respect to the tube-side gas flow. The feed-gas outlet VOC composition was monitored at definite time intervals.

Dimensionless Henry's law constants for four different VOCs were determined independently in two absorbent liquids (silicone oil and Partherm oil) by variable volume headspace technique (Poddar, 1995) using a headspace autosampler (Tekmar, Cincinnati, OH) interfaced with the Varian 3400 GC. Data for each VOC–absorbent oil combination were obtained at different temperatures.

Theoretical Considerations

To describe countercurrent absorption of a VOC species i in an absorbent in a membrane device of length L requires the solution of a split boundary-value problem involving the simultaneous solution of VOC mass-balance equations for the tube side (gas phase) and the shell side (liquid phase) coupled together by an equation for VOC diffusion (and permeation in the case of a skinned membrane) through the membrane wall. There is no analytical solution for this problem. The following strategy was adopted to simplify the numerical method used.

Consider a small segment of length $\Delta z = L/n$ at the device end ($z = 0$) where the gas exits; n is a large number (Figure 4). Assume the exiting gas concentration $C_{ig,\text{out}}$. The incom-

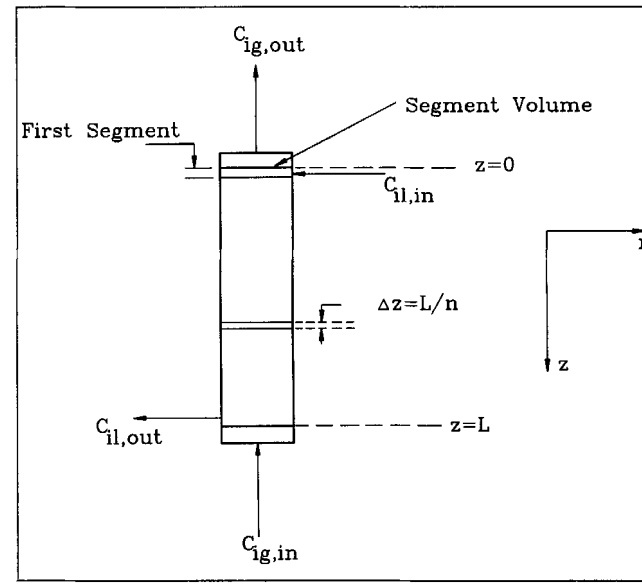

Figure 4. Absorption module for numerical simulation.

ing liquid phase concentration $C_{il,\text{in}}$ is known. If independent analytical expressions relating inlet and outlet concentrations for the gas phase and liquid phase, respectively, are developed for this segment, then one can find out the cup-mixing values of the inlet gas-phase concentration $\langle C_{ig}\rangle$ and liquid-outlet concentration $\langle C_{il}\rangle$ for the same segment. The same analytical expressions are then used for the next segment of length Δz: assume the gas-outlet concentration and liquid-inlet concentration to be equal to the gas-inlet concentration $\langle C_{ig}\rangle$ and liquid-outlet concentration $\langle C_{il}\rangle$, respectively, obtained from the previous segment. This procedure is repeated till the other end of the module is reached; the value of $\langle C_{ig}\rangle$ obtained for the last segment (at $z = L$) is compared with the known value of $C_{ig,\text{in}}$. If they are different, another guess of $C_{ig,\text{out}}$ at the top of the column ($z = 0$) is selected and the process is repeated till convergence is achieved. We now focus on the model and the development of the analytical expressions for the average gas-phase and liquid-phase concentrations at the end of the segment needed for implementing the iterative process described earlier.

Two types of hollow fibers have been employed; one has a porous wall and the other has a nonporous coating over a similar porous wall. Instead of developing a separate model for each type of fiber having a different fluid in the pores, a generalized model is adopted. Assume the pores to be filled with an imaginary fluid different from the gas in the tube side and absorbent in the shell side. The distribution coefficient of species i between the gas phase and the fluid phase inside the porous membrane is H_{i1}, while that between the absorbent liquid and the fluid inside the porous membrane is H_{i2}. The diffusivity of VOC species through this imaginary fluid inside the pore is D_{if}.

A model is needed also for the shell-side fluid flow. Because of the earlier successes of Happel's free surface model (Happel, 1959) in describing the complex shell-side flow in parallel-flow hollow-fiber modules (Gill and Bansal, 1973; Karoor and Sirkar, 1993), we adopt it here. It is assumed that the hollow fibers are distributed regularly; further each fiber is surrounded by an equal volume of liquid envelope whose boundary radius r_e (Figures 2a and 2b) is the free surface across which no mass, momentum, or energy transfer takes place. Analysis based on a single fiber may then be extended to the whole shell side of radius r_s containing N_f fibers

$$r_e = r_s/\sqrt{N_f}. \tag{5}$$

A set of nondimensional variables are introduced now:

$$\phi_{im} = \frac{C_{im}}{C_{ig,\text{in}}}; \qquad \phi_{ig} = \frac{C_{ig}}{C_{ig,\text{in}}}; \qquad \phi_{il} = \frac{C_{il}}{C_{ig,\text{in}}};$$

$$\xi = \frac{r}{r_i}; \qquad \zeta = \frac{z}{L}. \tag{6}$$

The governing balance equations and the boundary conditions are provided in Appendix A. The average gas-phase concentration at the inlet of the first segment Δz (at $z = 0$), $\langle \phi_{ig}\rangle$, and average liquid phase concentration at the outlet of the first segment Δz, $\langle \phi_{il}\rangle$, can be expressed by Eqs. 7 and 8, respectively (see Appendix A, Eq. A25 for derivation):

$$\langle \phi_{ig}\rangle = \frac{-2\pi\Delta_{ig}P}{n\lambda}\left(\phi_{im}|_{\xi_o} - H_{i1}\phi_{ig}|_{\xi=1}\right)\left(\frac{D_{ig}L}{\langle V_t\rangle}\right)_{\text{ref}} + \phi_{ig,\text{out}} \tag{7}$$

$$\langle \phi_{il}\rangle = \frac{-2\pi L D_{il} Q e'}{n\langle V_s\rangle[(A\xi_e/\xi_c) - B]}\left(\phi_{im}|_{\xi_o} - H_{i1}\phi_{ig}|_{\xi=1}\right) + \phi_{il,\text{in}}. \tag{8}$$

Here ϕ_{im} at $\xi_o (= r_o/r_i)$ and ϕ_{ig} at $\xi = 1$ are the nondimensional membrane-phase and gas-phase concentrations of VOC at the respective interfaces. These concentrations can be obtained by simultaneously solving the gas-phase (tube side), liquid-phase (shell side), and membrane-phase concentration profiles (for derivation see Appendix A after Eq. A24):

$$\phi_{im}|_{\xi_o} = \frac{\phi_{ig,\text{out}}[H_{i1}QY + (H_{i1}H_{i2}P/a)] + \phi_{il,\text{in}}(1 + 4PXH_{i1})}{QY + H_{i2}(1 + P/a + 4PXH_{i1})} \tag{9}$$

$$\phi_{ig}|_{\xi=1} = \frac{\phi_{ig,\text{out}}(QY + H_{i2} + H_{i2}P/a) + 4PX\phi_{il,\text{in}}}{QY + H_{i2}(1 + P/a + 4PXH_{i1})}. \tag{10}$$

Here a, P, Q, X, and Y are functions of physical properties such as gas diffusivity, liquid diffusivity, effective membrane diffusivity, membrane permeance, tortuosity, porosity and geometrical properties of the contactor; their expressions are given in Appendix A (Eqs. A19, A5, A20, A11 and A24). The effective diffusivity in the membrane phase D_{im} is given by (Prasad and Sirkar, 1988)

$$D_{im} = D_{if}\epsilon/\tau. \tag{11}$$

Case I — Absorption in porous fibers

The porous fiber has no coating; therefore, $\xi_c = \xi_0$, $\delta_c = 0$, and $a = \alpha$ (Eq. A19). Absorbent liquid wets the fiber and fills pores (Figure 2a). The pore fluid is identical to that in the shell side. Hence, $H_{i2} = 1$. H_{i1} is simply H_i, the Henry's law constant between the gas and the liquid phase. Further, $D_{if} = D_{il}$. It is also possible to show that the interfacial concentrations at ξ_o and ξ_c are identical.

Case II — Absorption in skinned fibers

Here absorbent liquid does not fill the pores due to the nonporous skin; hence, it is not in direct contact with the gas. Pores are gas-filled (Figure 2b). Hence, $H_{i1} = 1$. $H_{i2} = H_i$. D_{if} will be equal to the diffusivity of gaseous species i inside a straight pore, D_{igp}, defined later (in Eq. 20).

The gas phase encounters significant pressure drop even at lower flow rates due to the small fiber diameter. The volumetric gas flow rate per fiber, $\langle V_t\rangle$, is therefore reduced along the module length. For laminar flow, one can use the compressible form of Hagen–Poiseuille equation (Pan and Habgood, 1978) to calculate the pressure drop. The volumetric flow rate is assumed to be constant for the small segment of length Δz. The pressure at the upstream of the segment of

length Δz is obtained as a function of downstream pressure, p_{out}, as

$$p = [p_{out}^2 + (256\mu L p_{out}\langle V_{t,out}\rangle/\pi d_i^4 n)]^{1/2}. \quad (12)$$

The pressure and volumetric flow rate are then modified for the next segment. This procedure is followed for every segment till the module end is reached.

Estimation of physical parameters

Knowledge of VOC diffusivities in the absorbent liquid and other physicochemical properties are essential for obtaining numerical values from the mathematical model. Hutter et al. (1994) used the Wilke–Chang equation for calculating diffusivities of different VOCs in sunflower oil. The Wilke–Chang equation is valid for aqueous solutions and does not always give good predictions for organic solvents (Reid et al., 1977), especially those having high viscosity. Several investigators Hayduk and Cheng, 1971; Hiss and Cussler, 1973; Davis et al., 1967; Lusis, 1974) have shown that solute diffusivity in a viscous liquid varies inversely with the liquid viscosity raised to the power of some exponent, the value of which depends on the solute–solvent system. It was therefore decided to measure VOC diffusion coefficients in the absorbent liquid indirectly from the system.

Comparison of absorption Case I with the present mode of countercurrent sweep gas permeation (as discussed earlier) reveals that the calculation procedure for the absorption of Case I may be employed here with N_2 gas instead of the absorbent liquid passing through the shell side. The equations obtained in the VOC absorption analysis under Case I were therefore modified with appropriate conditions (Poddar, 1995). The liquid-phase concentration, ϕ_{il}, used in absorption is replaced by the sweep gas concentration ϕ_{isp}. In this case it is clear that $H_{i1} = H_{i2} = H_i$. There is no silicone coating, so $\xi_o = \xi_c$, and $a = \alpha$ (Eq. A19). At $\xi = \xi_o$, it is possible to write

$$\phi_{im}|_{\xi_o} = H_i \phi_{isp}|_{\xi_o}. \quad (13)$$

Using Eq. 13 one can find out the interfacial concentrations from Eqs. 9 and 10 as follows:

$$\phi_{isp}|_{\xi_o} = \frac{\phi_{ig,out} H_i QY + \phi_{isp,in}(1+4PXH_i)}{QYH_i + H_i^2(1+4PXH_i)} \quad (14)$$

$$\phi_{ig}|_{\xi=1} = \frac{\phi_{ig,out}(H_i + QY) + 4PX\phi_{isp,in}}{QY + H_i(1+4PXH_i)}. \quad (15)$$

Computational steps similar to the one used for predicting the outlet gas-phase concentration in absorption were employed to calculate D_{il} value. An arbitrary value of D_{il} was assumed here and $C_{ig,in}$ was calculated at the feed gas entrance. The calculated value of $C_{ig,in}$ was compared with the actual $C_{ig,in}$. The steps were repeated with different D_{il} values till the two inlet concentrations matched.

At a given pressure, the temperature dependence of Henry's law constant can be expressed by (Robbins et al., 1993; Hutter et al., 1994)

$$H_i = \exp[(B_{Hi}/T) - A_{Hi}], \quad (16)$$

where A_{Hi} and B_{Hi} are constants depending on the solvent–solute combination and need to be found out from experimental data (Poddar, 1995).

Permeance of a VOC through the composite membrane (skinned hollow fiber) can be calculated from the permeation-rate expression

$$w_i = (q_o/\delta_o) A_m (\Delta C_{i,p})_{lm}. \quad (17)$$

The gas-film mass-transfer resistances on both sides of the membrane are neglected. Due to low VOC concentrations, the VOC permeance (q_o/δ_o) is assumed to be independent of the VOC concentration. $(\Delta C_{i,p})_{lm}$, the logarithmic-mean concentration difference, is calculated from permeation experimental results in the conventional permeation mode (Guha et al., 1992). Once the overall permeance of a VOC through the composite membrane is known, the permeance through the silicone skin can be calculated from the following relation obtained from the resistances-in-series model:

$$\frac{\delta_o}{r_o q_o} = \frac{\delta_c}{(r_c)_{lm} q_c} + \frac{\delta_s}{(r_s)_{lm} D_{igp}}. \quad (18)$$

The diffusion coefficient of a VOC in a binary gas mixture (VOC-N_2) at low or moderate pressures was calculated from the following equation (Reid et al., 1977):

$$D_{ig} = 27.3051 \times 10^{-3} T^{3/2} [(M_i + M_{N_2})/M_i M_{N_2}]^{1/2} / p\sigma_{iN_2}^2 \Omega_D. \quad (19)$$

For Case II in the present study, pores are gas-filled. Information on diffusivity of VOC molecules inside the pores, D_{igp}, is required. For the system under study, the ratio of pore radius r_p to the mean free path λ_m is close to 0.1; slip flow is most likely to dominate inside the pores (Rangarajan et al., 1984). The expression for the corresponding diffusivity (Rangarajan et al., 1984) after necessary unit conversions is

$$D_{igp} = 1.0133 \times 10^6 r_p RT/M_i \bar{c}_i \quad (20)$$

where $\bar{c}_i$, the mean speed of the molecule, is given by

$$\bar{c}_i = (8.1064 \times 10^6 RT/\pi M_i)^{1/2}. \quad (21)$$

Results and Discussion

The reduction in the VOC concentration in the treated gas mixture as a function of the tube-side gas flow rate is illustrated in Figure 5. At low gas flow rates, a feed containing 999 ppmv of methylene chloride in N_2 can be purified to a level as low as 1–2 ppmv. Thus, 99.5%+ removal of methylene chloride is possible in a short microporous hollow-fiber countercurrent gas–liquid contactor using a *fresh absorbent.*

In the absorption model developed, the Graetz number appears in the denominator of the first term on the righthand

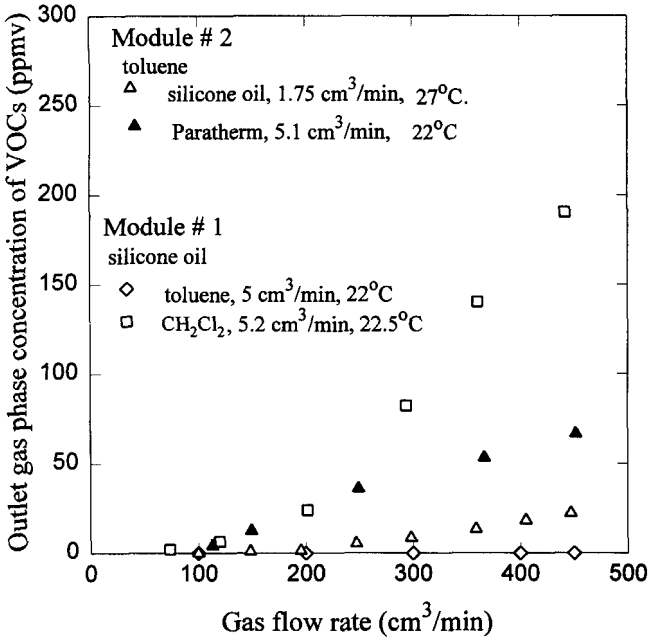

Figure 5. Variation of gas-phase VOC outlet concentration with gas flow rate for absorption of VOCs using porous fibers.

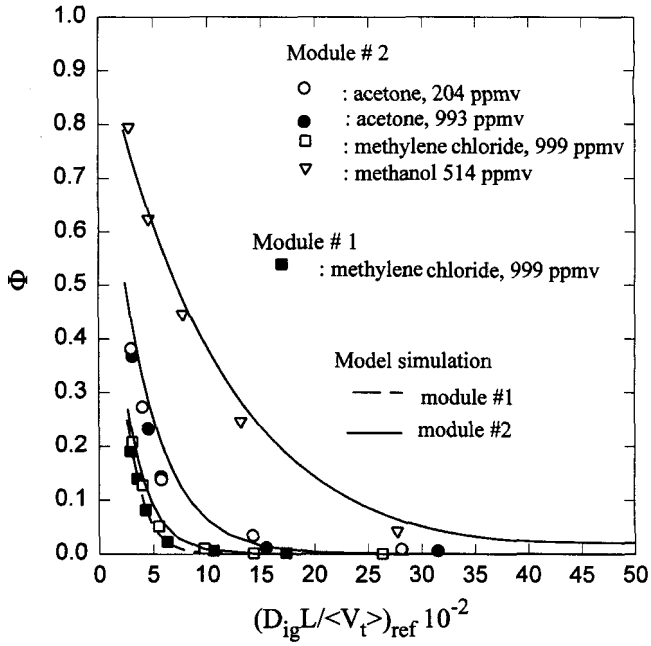

Figure 6. Ratio of outlet-to-inlet gas-phase concentration of different VOCs as a function of inverse of Graetz number.

side of the expression (Eq. 7) of average VOC concentration as $(\langle V_t\rangle/D_{ig}L)_{\text{ref}}$:

$$N_{Gz} = \frac{\pi r}{2L} N_{Re} N_{Sc} = \left(\frac{\langle V_t\rangle}{D_{ig}L}\right)_{\text{ref}}. \tag{22}$$

Experimental data and simulation plots of dimensionless exiting gas-phase concentration Φ ($=(C_{ig,\text{out}}/C_{ig,\text{in}}) = \phi_{ig,\text{out}}$, for the topmost segment only) for acetone, methanol, and methylene chloride absorption in silicone oil are compared in Figure 6 as a function of the inverse of Graetz number. For methylene chloride, experimental results from module 1 at higher gas flow rates as well as from module 2 at lower gas flow rates show very good agreement with model simulations. The simulation results for two modules differ slightly because Φ depends not only on the tube-side feed-gas-based Graetz number but also on the shell-side behavior (note that two modules have different fiber-packing fractions). For acetone, experimental results closely follow model predictions. Similar plots for toluene absorption in silicone oil and Paratherm are shown in Figure 7 for module 2.

Henry's law constants for the systems were calculated from Eq. 16. Constants A_{Hi} and B_{Hi} for different VOC-absorbent combinations were determined experimentally (Poddar, 1995). For all four VOCs, permeance through the composite membrane, q_o/δ_o, and permeance through the silicone skin, q_c/δ_c, are shown in Table 2. At higher VOC concentrations, Cha (1994) had observed a very strong dependence of VOC permeance on concentration. This dependence was ignored here since VOC concentrations are very low. Diffusivities of VOCs in the absorbent liquids, measured indirectly via VOC permeation experiments through the absorbent-filled porous membranes, are also provided in Table 2.

Highest VOC removal was achieved when the gas flow rate per fiber was low and around 0.1 cm^3/min/fiber. If the module is longer providing more gas–liquid (and, therefore, membrane) contact area, higher gas flow rates can be handled for equivalent VOC reduction. For lower fractional VOC absorption, say, 90%, a much higher gas flow rate of 0.4 cm^3/min/fiber can be maintained continuously. These numbers are useful for scaling up the VOC scrubber unless the

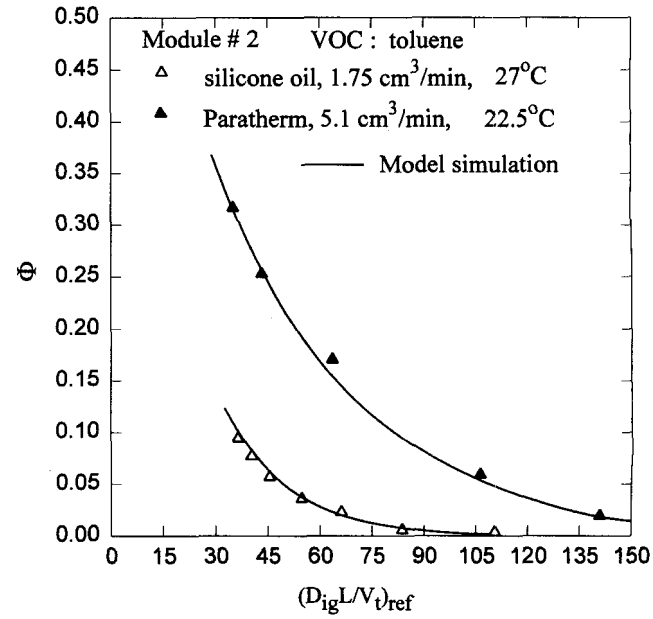

Figure 7. Ratio of outlet-to-inlet gas-phase concentration of toluene as a function of inverse of Graetz number.

Table 2. Diffusivity and Permeance Data for Various VOCs

VOC	Diffusivity (cm^2/s)		Permeance (cm/s)	
	Silicone Oil (50 cs)	Paratherm	Composite Membrane (q_o/δ_o)	Silicone Skin (q_c/δ_c)
Acetone	2.81×10^{-6}	3.60×10^{-7}	3.2×10^{-3}	3.22×10^{-3}
Methanol	4.71×10^{-6}	1.86×10^{-7}	2.89×10^{-3}	2.91×10^{-3}
Methylene chloride	4.30×10^{-6}	8.50×10^{-7}	5.01×10^{-3}	5.06×10^{-3}
Toluene	7.62×10^{-6}	4.80×10^{-6}	11.5×10^{-3}	11.7×10^{-3}

shell-side flow pattern changes substantially in a scaled-up module. Toluene is easily removed allowing a much higher gas flow rate per fiber (~1 cm^3/min/fiber). This value is reinforced by the results shown in Figure 5 for the larger module 1; virtually all of the toluene in the feed gas was removed even at higher flow rates.

For a given gas and absorbent flow rate, acetone percent removal remained independent of the feed composition as shown in Figure 8. Experimental results of methylene chloride and acetone removal by Paratherm and silicone oil in module 3 are reported in Figure 9. The outlet concentration of methylene chloride decreased strongly with decreasing gas flow rate. Unlike Figure 5, there was no direct gas–liquid contact here. However, the behavior was found to be similar. Removal performance of methylene chloride suggests that the difference in the diffusivities of methylene chloride in two different absorbents had no effect on their absorption performances. This issue is further discussed later.

As *proposed* in the Introduction, nondispersive gas absorption will not be achieved if the gas pressure is significantly higher than that of the liquid when the fiber has a nonporous skin or coating. Experimental evidence is provided in Figure 10 for N_2 gas passing through the tube side and Paratherm through the shell side. Initially both gas and liquid were kept at essentially atmospheric pressure. Under such conditions gas flow rates were measured at the module inlet and outlet. No measurable difference between the inlet and the outlet flow rates was observed. The same experiment was repeated at different higher gas pressures. As shown in Figure 10, outlet gas flow rates decreased as the gas pressure was increased. The difference in gas flow rates (though limited in amount) is the rate at which N_2 permeated through the silicone skin and bubbled through the absorbent in the shell side. The bubbling of N_2 through the translucent absorbent-filled outlet pipe was observed when gas pressure was higher than the liquid pressure. To stop this bubbling, it is essential to elevate the liquid side pressure to the level of gas-side pressure or higher. No bubbling was observed when both gas and liquid were at atmospheric pressure.

One may wrongly conclude now that there is no operational advantage of having a nonporous skin or coating since in either case (with or without coating) one of the phases has to be at a higher pressure unless both phases have the same pressure. For many VOC removal applications, the gas (N_2 or air) is at atmospheric pressure. If a microporous fiber without a nonporous coating is used, the gas pressure must be raised from atmospheric. This requirement is eliminated

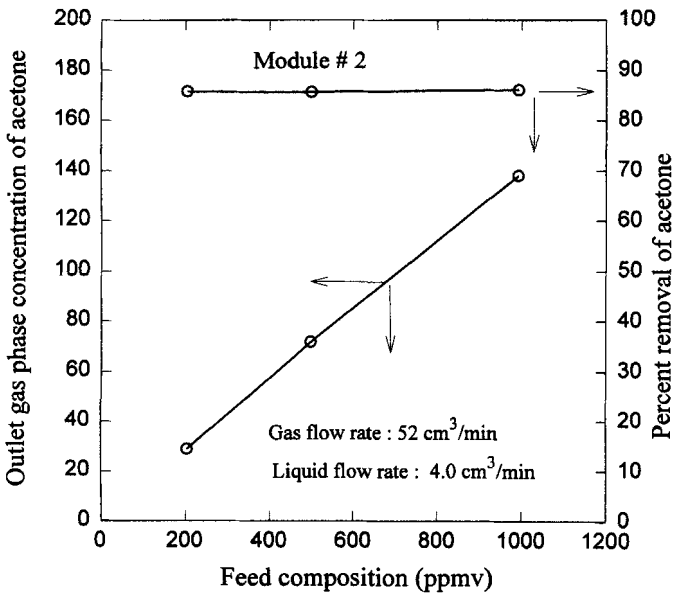

Figure 8. Variation of gas-phase VOC outlet concentration with feed-gas VOC composition for acetone absorption in silicone oil.

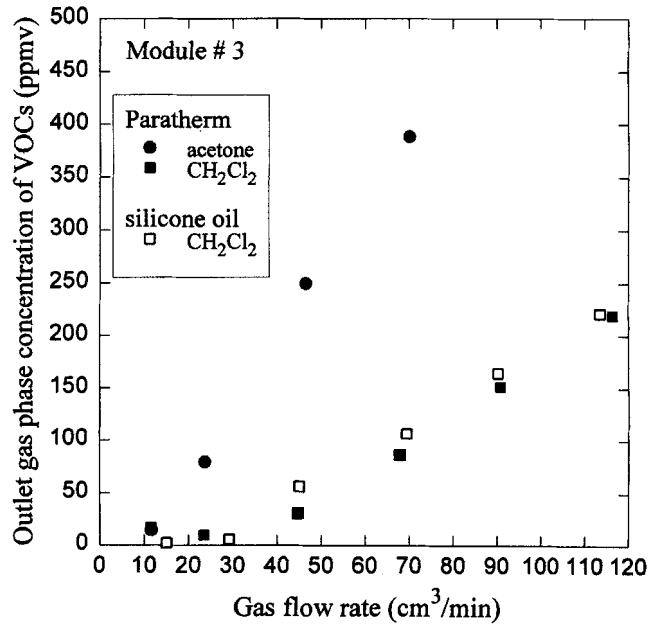

Figure 9. Variation of gas-phase VOC outlet concentration with gas flow rate for absorption of VOCs using skinned fibers.

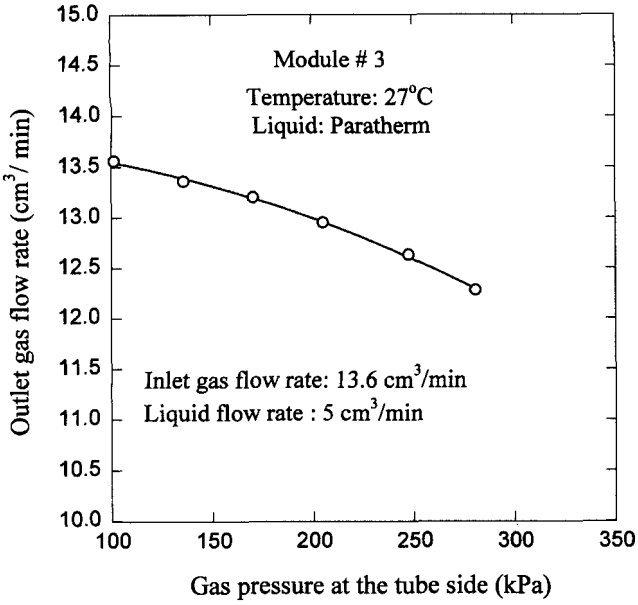

Figure 10. Nitrogen dispersion into absorbent liquid under adverse pressure condition in a fiber having nonporous silicone skin.

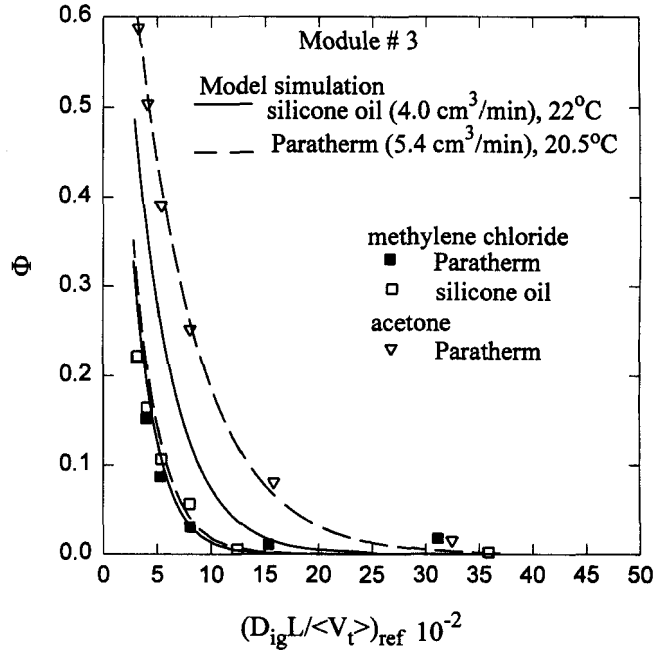

Figure 11. Ratio of outlet-to-inlet gas-phase concentration of methylene chloride and acetone as a function of inverse of Graetz number for absorption using skinned fiber with two different absorbents.

when a nonporous skin or coating is employed, resulting in considerable energy saving. Further, unlike microporous fibers, the skinned fibers allow absorption under conditions of high liquid pressure levels. The homogeneous silicone membrane on the outer surface of the hollow fiber was characterized via permeation of N_2 and CO_2. A selectivity value of 10–12 for CO_2 over N_2 was obtained (Poddar, 1995) that is comparable to the literature value for silicone rubber (Robb, 1965).

Figure 11 illustrates the variation of Φ vs. inverse of Graetz number in a skinned fiber module for absorption in silicone oil and Paratherm. For methylene chloride, both absorbents show almost identical performance as observed from the data and model predictions. This indicates that the difference in the diffusivities of the two absorbents does not control absorption of methylene chloride. It is the skin resistance that controls the performance. However, this cannot be generalized for the absorption of any VOC using skinned fiber module. Simulation plots for acetone absorption using skinned fibers (Figure 11) illustrate the considerable effect of the characteristics of the absorbent flowing through the shell side.

We now focus on the effect of gas and liquid flow rates on the mass-transfer coefficients. The overall gas-phase-based mass-transfer coefficient (K_{oG}) values at a given liquid flow rate in porous fiber modules were plotted against gas flow rate/fiber for individual VOCs in Figure 12. K_{oG} became independent at a relatively higher gas flow rate (~0.5 cm³/min/fiber). This plateau value is determined by the resistance of VOC diffusion through the stagnant absorbent in the membrane pores and in the flowing absorbent liquid. As expected from Figures 5, 6, and 7, toluene shows the highest K_{oG} values followed by methylene chloride, acetone, and methanol. The superior mass-transfer characteristics of toluene are due to the higher Henry's law constant and diffusivity value. Figure 13 shows how K_{oG} varies with the absorbent-liquid flow rate for methylene chloride and toluene. It became essentially constant beyond 5 cm³/min/fiber of liquid flow rate for both VOCs. Variation of Φ as a function of the absorbent flow rate has also been predicted by the model. As shown in Figure 14, these model-predicted values compare quite well with the experimental results.

Mass-transfer characteristics of methylene chloride absorption are shown in Figure 15 for two different fibers and two different absorbents. Experiments were carried out under essentially identical conditions. The porous fiber has a much

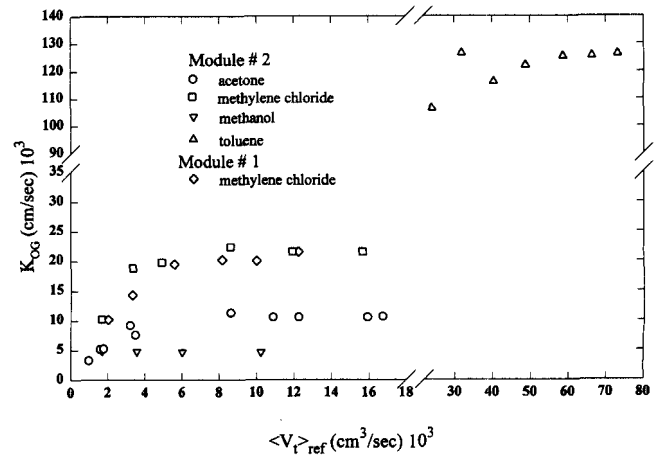

Figure 12. Variation of gas-phase-based overall mass-transfer coefficient with gas flow rate per fiber for absorption of different VOCs in silicone oil using porous fibers.

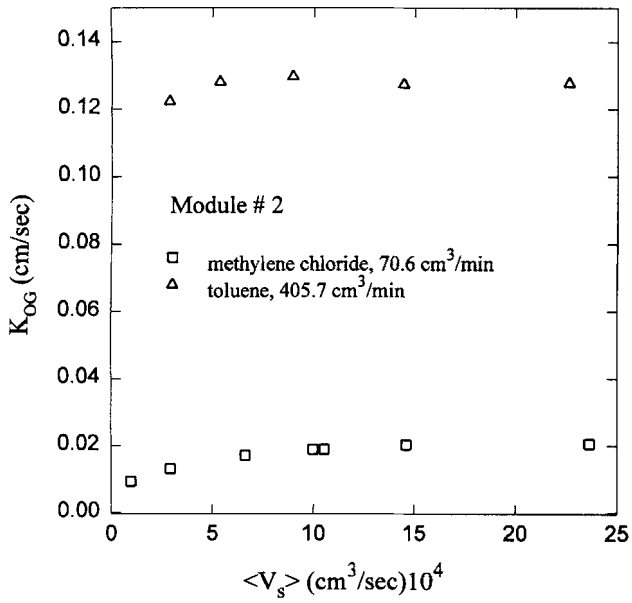

Figure 13. Variation of gas-phase-based overall mass-transfer coefficient with absorbent liquid flow rate per fiber for VOC absorption in silicone oil using porous fibers.

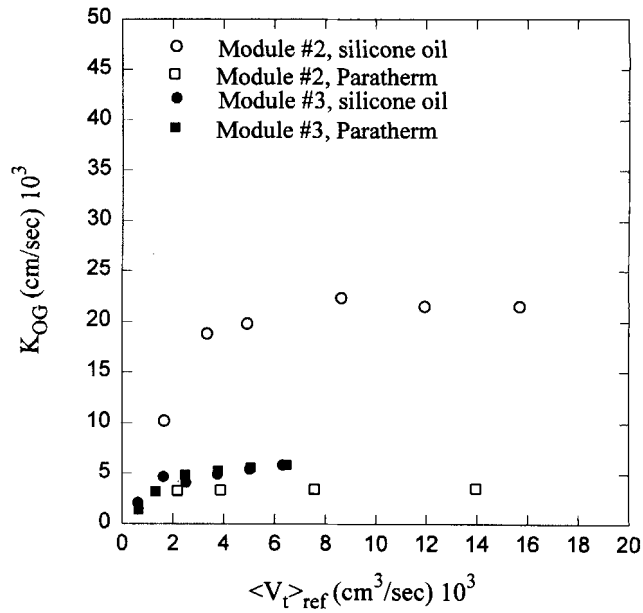

Figure 15. Mass-transfer characteristics of methylene chloride absorption between two different absorbents and two different fibers.

higher K_{oG} than the skinned fiber for silicone oil. Although silicone oil yields much higher K_{oG} than Paratherm for porous fibers, the same is not true for the skinned fiber.

In absorption with porous fibers, the membrane pores are filled with the absorbent oil. Resistance to VOC transfer through this immobilized absorbent *appears to control* the overall mass transfer *at higher gas and liquid flow rates*. For a given system, the membrane mass-transfer coefficient is directly proportional to the diffusivity of the VOC through the absorbent inside the pore. Since methylene chloride has a much lower diffusivity in Paratherm than in silicone oil, the overall mass-transfer coefficient is lower for Paratherm. The substrate pores remain gas-filled for absorption using skinned fibers, and mass-transfer characteristics of VOC absorption in such fibers are *probably* controlled by the resistance of VOC permeation through the silicone skin. That is why the overall mass-transfer coefficient for methylene chloride absorption is apparently independent of the nature of absorbent used for the given skinned fiber.

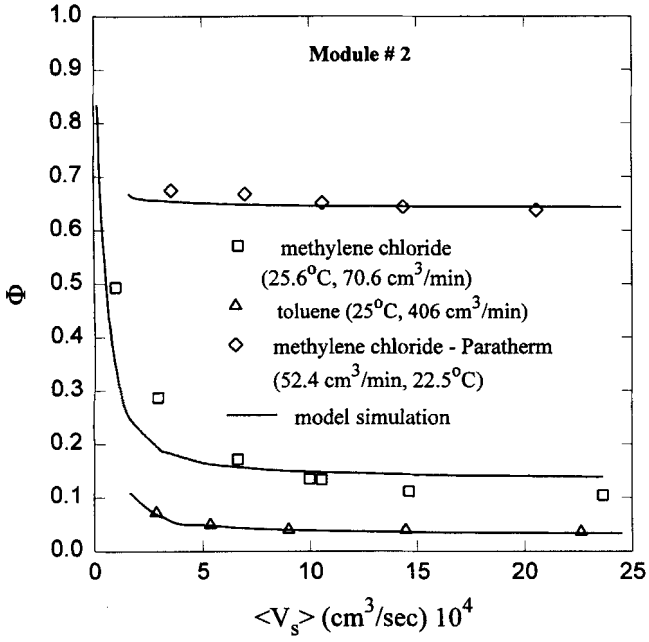

Figure 14. Ratio of outlet-to-inlet gas-phase concentration of VOCs as a function of liquid flow rate.

The overall mass-transfer coefficient may be related to the individual mass-transfer coefficients by the resistances-in-series model. For the porous fiber

$$R_{oG} = \frac{1}{K_{oG}} = \frac{1}{k_g} + \frac{d_i}{H_i d_{lm} k_m} + \frac{d_i}{H_i d_o k_l}. \quad (23)$$

Here, k_m is the mass-transfer coefficient through the absorbent-filled porous membrane and can be expressed as (Prasad and Sirkar, 1988)

$$k_m = D_{il}\epsilon/\tau(r_o - r_i). \quad (24)$$

For the skinned fiber

$$R_{oG} = \frac{1}{K_{oG}} = \frac{d_o}{k_g d_i} + \frac{d_o}{(d_s)_{lm} k_m} + \frac{d_o}{(d_c)_{lm} k_c} + \frac{d_o}{H_i d_c k_l}. \quad (25)$$

Here, k_m is the gas-filled substrate mass-transfer coefficient

$$k_m = D_{igp}\epsilon/\tau(r_o - r_i). \quad (26)$$

Table 3. Membrane Resistances for Absorption of Different VOCs Using Porous Fiber

VOC	Absorbent	T °C	$D_{il} \times 10^6$ cm^2/s	H_i	k_m cm/s $\times 10^4$	R_m s/cm	R_{oG} s/cm	R_m/R_{oG}
Acetone	Silicone oil	22.0	2.81	61.49	1.37	98.05	100.00	0.98
Methanol	Silicone oil	22.2	6.11	17.62	2.26	203.6	213.7	0.95
Methylene chloride	Silicone oil	22.0	4.30	90.72	2.06	43.3	47.62	0.91
Toluene	Silicone oil	27.0	7.62	342.6	3.66	6.47	7.94	0.81
Methylene chloride	Paratherm	22.5	0.85	76.5	0.41	259.8	281.7	0.92
Toluene	Paratherm	22.0	4.80	229.2	2.30	15.4	18.5	0.83

The mass-transfer coefficient through the silicone skin is the VOC permeance through the skin:

$$k_c = q_c/\delta_c. \tag{27}$$

Table 3 shows the overall mass-transfer resistance and the absorbent-filled membrane resistance for different VOC absorptions in silicone oil and Paratherm in the porous fiber module. Total resistance was calculated as the inverse of the averaged maximum values of K_{oG} obtained from averaged plateau values (as in Figure 12). Note that the ratio of the absorbent-filled membrane resistance to the total resistance of mass transfer is quite large and can be as high as 0.98 (for acetone) or 0.8 (for toluene). Similar results for the skinned fibers are shown in Table 4 for two VOCs (acetone and methylene chloride). The silicone skin resistance is inversely proportional to the VOC permeance through the skin. Despite having a lower diffusion coefficient, Paratherm appears to provide a higher mass-transfer coefficient than silicone oil for methylene chloride absorption due to the higher Paratherm flow rate (5.4 cm^3/min compared to 4.0 cm^3/min for silicone oil). It was observed that the mass-transfer coefficient attained a plateau at a liquid flow rate 5 cm^3/min or higher in module 2.

It is clear from Figure 15 that the skin resistance controlled the mass-transfer rate for methylene chloride absorption, that is, skin resistance to overall resistance ratio was very high (close to unity). However, ratios slightly higher than unity were also observed in Table 4. This is apparently contrary to reality. Skin resistance for a particular VOC was calculated based on the permeance value obtained from experiments using dry skinned hollow fiber. In the absorption experiments, organic liquid (silicone oil or Paratherm) flowing through the shell side caused possible swelling of the silicone skin and thus decreased the skin resistance for mass transfer. Data for methylene chloride in Table 4 can be explained by this swelling phenomenon. The ratio of the skin resistance to the overall resistance is much less for acetone absorption, only 0.64. This clearly indicates that *skin resistance control cannot be taken for granted.* It will depend on the relative contributions of permeation through the skin and diffusion in the shell-side boundary layer for a given VOC-absorbent system.

These results and analysis are useful for a *short-cut design* of modules using currently available porous hollow fibers for VOC absorption in organic absorbents that wet the fiber. From Table 3, it appears that more than 80% of the total resistance to mass transfer for VOC absorption in a porous fiber module is due to the membrane. These numbers are obtained at *higher gas and liquid flow rates* where the overall mass-transfer coefficient becomes almost independent of the gas and liquid flow rates. *To develop a preliminary design* for a porous fiber-based absorption module, there is no need for highly reliable gas-phase (tube-side) or liquid-phase (shell-side) mass-transfer coefficient correlations. The membrane resistance or mass-transfer coefficient can be readily calculated from Eq. 24 using known parameters. For all practical purposes, this resistance may be assumed to be 80% (a conservative value) of the total resistance to calculate the area required for a given VOC absorption system design. The gas flow rate should be more than 0.5 cm^3/min/fiber, and a liquid rate of 0.05 cm^3/min/fiber or more is recommended with appropriate allowance for membrane length. Note, however, these values are highly VOC-dependent, especially the gas flow rate, for VOCs having higher H_i, for example, toluene.

Absorption of multiple VOCs from a N_2 gas stream have been carried out to a limited extent. Table 5 provides the Paratherm-based absorption data for two flow rates of a N_2 stream containing four VOCs in module 3. High rates of removal of all VOCs except the highly polar methanol were observed. The removal of a particular VOC from a mixture appears to be somewhat inferior to that from a single VOC-N_2 mixture.

A continuous process for VOC absorption from N_2/air into an absorbent via either of two different kinds of hollow fiber membranes requires simultaneous regeneration of the spent absorbent in a VOC stripper. In this study, membrane module 2 was used as the VOC absorber (where the gas pressure was slightly higher than that of the absorbent) along with membrane module 3 as the VOC stripper (and, therefore, an

Table 4. Skin Resistances for Absorption of VOCs using Skinned Hollow Fiber

VOC	Absorbent	k_c cm/s	R_c s/cm	K_{oG} cm/s	R_{oG} s/cm	R_c/R_{oG}
Acetone	Paratherm	0.00322	309.5	2.07×10^{-3}	483.1	0.64
Methylene chloride	Silicone oil	0.00506	196.7	5.38×10^{-3}	185.8	1.06
Methylene chloride	Paratherm	0.00506	196.7	5.58×10^{-3}	179.2	1.1

Table 5. Absorption Data for a Mixed VOC-N_2 Gas Mixture*

VOC Concentration in Inlet N_2 Gas Stream ppmv		Gas Flow Rate (cm^3/min) 11.7 Outlet Conc. ppmv	11.7 Removal %	34.1 Outlet Conc. ppmv	34.1 Removal %
Acetone	226	14	93.8	87	61.5
Methylene chloride	201	9	95.5	18	91.0
Toluene	204	0.00	100.0	0.00	100.0
Methanol	163	77	52.7	128	21.5
Total	794	100	87.4	233	70.6

*Module 3; absorbent: Paratherm NF™; liquid flow rate: 5.6 cm^3/min; temperature: 22°C.

absorbent regenerator). In module 2, the flow arrangement was similar to that used in simple absorption experiments; full vacuum was applied to the fiber bore in module 3 to remove the VOC from the absorbent flowing on the shell side of module 3 on a continuous basis. The actual level of pressure could not be monitored due to the sensitivity limitations of the vacuum gauge. Results for methylene chloride removal from N_2 by simultaneous absorption and stripping (Figure 1) using silicone oil are shown in Figure 16. It was observed that a feed containing 999 ppmv of methylene chloride was purified continuously to around 20 ppmv when the feed flow rate was low. Many more successful experiments have been done over extended periods; these results and a suitable model describing the results have been communicated elsewhere (Poddar et al., 1996).

In the experiments with Paratherm or silicone oil, no peaks of the vapors of these absorbents were observed in the exit gas stream GC analysis. Paratherm is known to be stable over long lengths of time. Possessing a relatively higher vapor pressure (reported), silicone oil, however, slowly starts deteriorating after about eighteen months. We have also used such a degraded silicone oil as an absorbent flowing in the microporous hollow fiber module and observed small peaks in the GC.

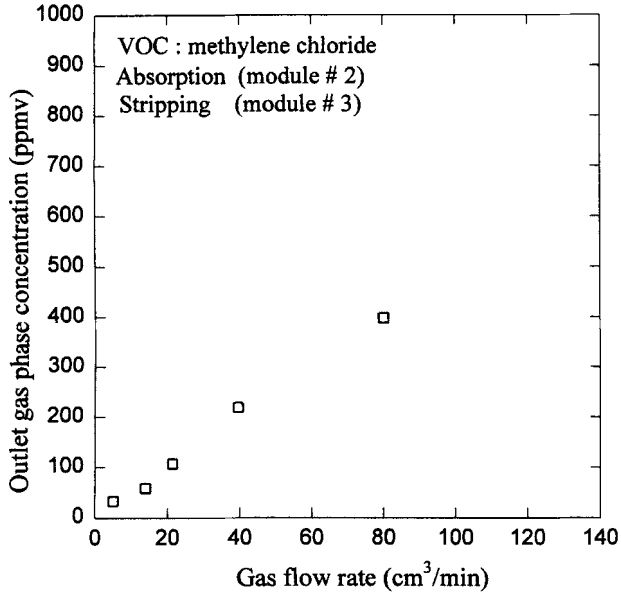

Figure 16. Steady-state outlet concentration vs. gas flow rate for simultaneous absorption and stripping of methylene chloride.

Absorption experiments show in general good agreements with model simulation results. At higher gas flow rates, a maximum deviation of 10% to 15% was observed between experimental and simulation results for Φ. However, the deviations between the two results are much more (50% to 60%) when the gas flow rates were very low (0.1 cm^3/min/fiber or less). The exiting VOC concentrations are very low at lower gas flow rates; hence, the deviations are not clear in the plots. However, their relative magnitude is high. One should look at such deviations from a different perspective. It is necessary to compare the total amount or percent of VOC removed from feed gas at low gas flow rates. For example, if a feed mixture containing 999 ppmv VOC is brought down to 6 ppmv and the model predicts 4 ppmv, the model is quite successful, yet direct comparison of Φs will indicate a large deviation. Further, VOC absorption at lower gas flow rates per fiber is not economical because the overall mass-transfer coefficient will be lower. It would be economical to design the absorber module for higher gas flow rates per fiber to take advantage of the higher values of K_{oG}. At higher gas flow rates, concentration of VOC can be brought to a low level by increasing the module length.

Overall gas-phase-based mass-transfer coefficient, K_{oG}, and the volumetric mass-transfer coefficient, $K_{oG}a$, were calculated for methylene chloride absorption with silicone oil in a conventional packed bed (Treybal, 1980). Results of calculations for different liquid-to-gas flow rate ratios are shown in Table 6. Higher $K_{oG}a$ values were obtained for higher liquid to gas flow rate ratios. For high levels of purification, it is not possible to design a packed tower with a very high liquid-to-gas flow rate ratio due to flooding. Moreover there are no correlations in literature for higher liquid-to-gas flow rate ratios. This problem does not arise in hollow-fiber-based operation. Even for the low packing density of 29.8 cm^2/cm^3 in module 2, ratios for $K_{oG}a$ values between module 2 and the packed tower are quite large. Further improvement of the membrane module performance is possible by having transverse liquid flow with baffles in the shell side and by introducing fibers having higher porosity (e.g., Celgard X-20), lower tortuosity, and thinner membrane wall.

Concluding Remarks

VOCs were efficiently removed from a nitrogen stream to potentially very low levels by absorption in an inert non-

Table 6. Volumetric Mass-Transfer Coefficients: Hollow-Fiber Modules vs. Packed Bed for Methylene Chloride Absorption in Silicone Oil

G'**	L'/G'	D_T	k_g	$k_i^* \times 10^3$	$(K_{oG})_{PT}$	$(a)_{PT}$	$(K_{oG}a)_{PT}$	$(K_{oG}a)_{HFM}/(K_{oG}a)_{PT}$ 1	2
32.94	5	30.48	1.202	3.93	0.257	0.53	0.137	10.5	4.8
65.88	10	42.0	1.303	5.49	0.338	0.68	0.231	6.3	2.8
16.47	20	27.0	1.416	5.98	0.368	0.71	0.262	5.6	2.5

** Units of all quantities are provided in the Notation.
Temperature: 25°C; H_i: 83.3; packing: 13-mm Berl saddles; pressure drop: 0.400 kPa.
PT: Packed tower. *HFM*: Hollow-fiber module.
1: module 1; $a = 66.67$ cm^2/cm^3.
2: module 2; $a = 29.8$ cm^2/cm^3.

volatile organic absorbent in a hollow-fiber membrane module. Spent absorbent liquid was regenerated in a separate coated hollow-fiber stripper by applying vacuum through the tube side and recycled back to the absorber. For a given absorbent and process conditions, absorption efficiency depended strongly on the VOC. Toluene displayed the highest absorption rate among all four VOCs, followed by methylene chloride, acetone, and methanol, in that order. For a given VOC and process conditions, silicone oil provided higher removal efficiency than Paratherm due to higher VOC diffusivity and Henry's law constant values in silicone oil. However, Paratherm appeared to be better for long-term stability. For absorption using porous hydrophobic hollow fibers, a stable gas–liquid interface can be created at the pore mouth on the gas side of the fiber by maintaining gas-side pressure higher than the liquid-side pressure to achieve nondispersive gas absorption. The absorbent-filled porous membrane wall contributed about 80–95% of the total resistance to mass transfer at relatively higher gas and liquid flow rates. For absorption using skinned fibers, it is essential to maintain the liquid-side pressure equal to or higher than the gas-side pressure. Mass-transfer characteristics appeared to be controlled primarily by the silicone skin resistance and the resistance of the absorbent liquid film outside the fiber. Comparison of VOC absorption characteristics between the porous and skinned fiber reveals that the relative performance of the two types of fiber for a given VOC absorption depends on the diffusivity of the VOC in the absorbent liquid used. Experimental results plotted as dimensionless concentration against the inverse of the tube-side gas-flow-based Graetz number demonstrated good agreement with predictions from the mathematical model. The volumetric mass-transfer coefficient in hollow-fiber contactors was found to be much higher than that in packed towers. Such a regenerative absorption process can potentially replace activated carbon adsorption-based processes.

Acknowledgment

The financial support of the Hazardous Substance Management Research Center at New Jersey Institute of Technology, Newark, is gratefully acknowledged. We thank Hoechst Celanese Separations Products, Charlotte, NC, for generously supplying us with Celgard fibers. We are also grateful to Applied Membrane Technology Inc., Minnetonka, MN, for the supply of the coated fibers.

Notation

a = mass-transfer surface area per unit volume, cm^2/cm^3
A_m = membrane area based on ID of porous fiber and OD of skinned fiber, cm^2
C_i = local concentration of species i, mol/cm^3
d_i = inside diameter of the hollow fiber, cm
D_{im} = diffusivity of species i in absorbent-filled membrane phase, cm^2/s
D_T = packed tower diameter, cm
G' = gas flow rate in packed tower, g/s
k = mass-transfer coefficient of an individual phase, cm/s
L' = liquid flow rate in packed tower, g/s
M_i = molecular weight of gaseous species i, g/mol
p_i = partial pressure of VOC species i
q_c = permeability of VOC through the silicone skin, cm^2/s
q_o = overall permeability of VOC through composite membrane, cm^2/s
r_i, r_c = inside radius of the fiber, outside radius of the coated fiber, respectively, cm
r_o = outside radius of the porous substrate, cm
$(r_s)_{lm}$ = logarithmic mean of r_o and r_i, cm
$(r_c)_{lm}$ = logarithmic mean of r_c and r_o
R = universal gas constant, resistance to mass transfer
T = temperature, K
$\langle v_{zs} \rangle$ = average velocity of liquid in the shell side per fiber, cm/s
$\langle v_{zt} \rangle$ = average velocity of gas inside the tube per fiber, cm/s

Greek letters

δ = thickness of the membrane, cm
$\Delta_{ig} = D_{ig}/(D_{ig})_{\text{ref}}$
ϵ = surface porosity of porous membrane
μ = viscosity of gas, g/cm·s
ϕ_i = dimensionless concentration of species i, Eq. 6
$\langle \phi_i \rangle$ = average dimensionless concentration of species i
ζ = dimensionless axial distance, defined in Eq. 6
$\lambda = \langle v_{zt} \rangle / \langle v_{zt} \rangle_{\text{ref}} = \langle V_t \rangle / \langle V_t \rangle_{\text{ref}}$
ξ = dimensionless radius, Eq. 6
Φ = ratio of treated gas-phase VOC concentration to inlet concentration
τ = tortuosity of the porous membrane

Subscripts

o = outside of the porous fiber, overall composite membrane
c = nonporous silicone skin
s = shell side, porous substrate
t = tube side

Literature Cited

Armand, B. L., H. B. Uddholm, and P. T. Vikstrom, "Absorption Method to Clean Solvent-Contaminated Process Air," *Ind. Eng. Chem. Res.*, **19**, 436 (1990).
Baker, R. W., C. M. Bell, and H. Wijmans, "On Membrane Vapor Separation versus Carbon Absorption," AIChE Meeting, San Francisco (1989).
Bird, R. B., W. E. Stewart, and E. N. Lightfoot, *Transport Phenomena*, Wiley, New York, p. 296 (1960).
Cha, J. S., "Removal of Vapors from Air by Selective Membrane Processes," PhD Diss., New Jersey Inst. of Technology, Newark (1994).

Davis, G. A., A. B. Ponter, and K. Craine, "The Diffusion of Carbon Dioxide in Organic Liquids," *Can. J. Chem. Eng.*, **45**, 372 (1967).
Gill, W. N., and B. Bansal, "Hollow Fiber Reverse Osmosis Systems Analysis and Design," *AIChE J.*, **19**(4), 823 (1973).
Guha, A. K., S. Majumdar, and K. K. Sirkar, "Gas Separation Modes in a Hollow Fiber Contained Liquid Membrane Permeator," *Ind. Eng. Chem. Res.*, **31**, 593 (1992).
Happel, J., "Viscous Flow Relative to Arrays of Cylinders," *AIChE J.*, **5**(2), 174 (1959).
Hayduk, W., and S. C. Cheng, "Review of Relation between Diffusivity and Solvent Viscosity in Dilute Liquid Solutions," *Chem. Eng. Sci.*, **26**, 635 (1971).
Hiss, T. G., and E. L. Cussler, "Diffusion in High Viscosity Liquids," *AIChE J.*, **19**, 698 (1973).
Hutter, J. C., G. F. Vandegrift, L. N. Nunez, and D. H. Redfield, "Removal of VOCs from Groundwater using Membrane-Assisted Solvent Extraction," *AIChE J.*, **40**(1), 166 (1994).
Jansen, A. E., P. H. M. Feron, J. J. Akkerhuis, and B. P. T. Meulen, "Vapor Recovery from Air with Selective Membrane Absorption," ICOM'93, Heidelberg, Germany (1993).
Karoor, S., and K. K. Sirkar, "Gas Absorption Studies in Microporous Hollow Fiber Membrane Modules," *Ind. Eng. Chem. Res.*, **32**, 674 (1993).
Kvaerner Engineering, Sanderfjord, Norway, Letter to K. K. Sirkar (Nov. 15, 1993).
Lusis, M. A., Letter to the Editor, *AIChE J.*, **20**, 207 (1974).
Mukhopadhyay, N., and E. C. Moretti, "Current and Potential Future Industrial Practices for Reducing and Controlling Volatile Organic Compounds," *CWRT*, AIChE (1993).
Pan, C. Y., and H. W. Habgood, "Gas Separation by Permeation," *Can. J. Chem. Eng.*, **56**, 210 (1978).
Peinemann, K. V., J. M. Mohr, and R. W. Baker, "The Separation of Organic Vapors from Air," *AIChE. Symp. Ser.*, **82**(250), 19 (1986).
Poddar, T. K., "Removal of VOCs from Air by Absorption and Stripping in Hollow Fiber Devices," PhD Diss., New Jersey Inst. of Technology, Newark (1995).
Poddar, T. K., S. Majumdar, and K. K. Sirkar, "Removal VOCs from Air by Membrane-based Absorption and Stripping," *J. Memb. Sci.*, in press (1996).
Prasad, R., and K. K. Sirkar, "Dispersion-Free Solvent Extraction with Microporous Hollow Fiber Modules," *AIChE J.*, **34**(2), 177 (1988).
Rangarajan, R., M. A. Mazid, T. Matsuura, and S. Sourirajan, "Permeation of Pure Gases under Pressure through Asymmetric Porous Membranes: Membrane Characterization and Prediction of Performance," *Ind. Eng. Chem. Process Des. Dev.*, **23**, 79 (1984).
Reid, R. C., J. M. Prausnitz, and T. K. Sherwood, *The Properties of Gases and Liquids*, 3rd ed., McGraw-Hill, New York (1977).
Robb, W. L., "The Silicone Membranes—Their Permeation Properties and Some Applications," *General Electric Res. and Dev. Center*, Rep. 65-C-301 (1965).
Robbins, G. A., S. Wang, and J. D. Stuart, "Using the Static Headspace Method to Determine Henry's Law Constants," *Anal. Chem.*, **65**, 3113 (1993).
Semmens, M. J., R. Qin, and A. Zander, "Using a Microporous Hollow Fiber Membrane to Separate VOCs from Water," *J. AWWA*, **81**, 162 (1989).
Skelland, A. H. P., *Diffusional Mass Transfer*, Wiley, New York (1973).
Treybal, R. E., *Mass-Transfer Operations*, 3rd ed., McGraw-Hill, New York, p. 200 (1980).
Zhang, Q., and E. L. Cussler, "Microporous Hollow Fibers for Gas Absorption: I. Mass Transfer in the Liquid," *J. Mem. Sci.*, **23**, 321 (1985).

Appendix A

In the model, the following assumptions are employed: steady state, isothermal conditions, constant absorbent viscosity, constant VOC diffusivity in the absorbent, fully developed concentration profiles in tube side and shell side, no axial diffusion in either side, no convective VOC transport in the fluid-filled membrane phase, no pressure drop for the absorbent liquid, negligible solubility of N_2 in absorbent, low VOC concentration in the gas phase (i.e., molar gas flow rate through fiber bores remains essentially constant), and applicability of Henry's law. The differential mass balance equation for the VOC species i in the stagnant fluid inside the membrane pore is

$$D_{im}\frac{1}{\xi}\frac{\partial}{\partial\xi}\left(\xi\frac{\partial\phi_{im}}{\partial\xi}\right)=0 \qquad 0\le\xi\le 1. \tag{A1}$$

Following are the boundary conditions used to solve this membrane phase equation:

$$\xi=1, \qquad \phi_{im}|_{\xi=1}=H_{i1}\phi_{ig}|_{\xi=1} \tag{A2}$$

$$\xi=1, \qquad D_{im}\left(\frac{\partial\phi_{im}}{\partial\xi}\right)_{\xi=1}=D_{ig}\left(\frac{\partial\phi_{ig}}{\partial\xi}\right)_{\xi=1}. \tag{A3}$$

The solution of Eq. A1 (Poddar, 1995) can be rearranged at the location ξ_o (i.e., $\phi_{im}=\phi_{im}|_{\xi_o}$) as follows:

$$\left(\frac{\partial\phi_{ig}}{\partial\xi}\right)_{\xi=1}=P(\phi_{im}|_{\xi_o}-H_{i1}\phi_{ig}|_{\xi=1}) \tag{A4}$$

$$P=(D_{im}/D_{ig})/\ln\,\xi_o. \tag{A5}$$

For fully developed laminar gas-phase flow in the tube side (parabolic velocity profile), the differential mass balance equation for VOC species i can be written as

$$\frac{1}{\xi}\frac{\partial}{\partial\xi}\left(\xi\frac{\partial\phi_{ig}}{\partial\xi}\right)=-\frac{\lambda}{\Delta_{ig}}\left(\frac{2\langle V_t\rangle}{\pi D_{ig}L}\right)_{\text{ref}}(1-\xi^2)\left(\frac{\partial\phi_{ig}}{\partial\zeta}\right) \qquad 0\le\xi\le 1. \tag{A6}$$

Here "ref" indicates the conditions for gas flow measurement, that is, atmospheric pressure and room temperature at the module exit. Equation A6 has to be solved with the following boundary conditions in the small column segment of length $\Delta z\ (=L/n)$ at $z=0$:

$$\xi=0, \qquad (\partial\phi_{ig}/\partial\xi)=0 \tag{A7}$$

$$\xi=1, \qquad (\partial\phi_{ig}/\partial\xi)|_{\xi=1}=\frac{D_{im}}{D_{ig}}(\partial\phi_{im}/\partial\xi)|_{\xi=1}=P(\phi_{im}|_{\xi_o}-H_{i1}\phi_{ig}|_{\xi=1}). \tag{A8}$$

The expression for boundary condition A8 is obtained from Eq. A4. A simple mass balance for the segment of length Δz at $z=0$ can be used as the third boundary condition (Bird et al., 1960):

$$-\frac{2\pi L}{n}\left(D_{ig}\frac{\partial\phi_{ig}}{\partial\xi}|_{\xi=1}\right)=4\pi r_i^2\int_0^1(\phi_{ig}-\phi_{ig,\text{out}})<v_{zt}>(1-\xi^2)\xi\,d\xi. \tag{A9}$$

For a fully developed concentration profile, $(\partial\phi_{ig}/\partial\zeta)_\xi$ is assumed not to be a function of ξ (Skelland, 1973). Hence, with the help of boundary conditions A7, A8, and A9, the solution of Eq. A6 can be obtained (Poddar, 1995) and written at $\xi = 1$ as

$$(1+4PXH_{i1})\phi_{ig}|_{\xi=1} - 4PX\phi_{im}|_{\xi_o} - \phi_{ig,\text{out}} = 0 \quad \text{(A10)}$$

where

$$X = \frac{11}{96} - \frac{\pi\Delta_{ig}}{2n\lambda}(D_{ig}L/\langle V_t\rangle)_{\text{ref}}. \quad \text{(A11)}$$

The shell-side conservation equation for species i in the liquid is similar to that in the tube side:

$$D_{il}\frac{1}{\xi}\frac{\partial}{\partial\xi}\left(\xi\frac{\partial\phi_{il}}{\partial\xi}\right) = v_{zs}(\xi)\frac{\partial\phi_{il}}{\partial\zeta} \qquad \xi_c \le \xi \le \xi_e. \quad \text{(A12)}$$

For fully developed laminar absorbent flow through the cylindrical annular space (Figures 2a and 2b), the velocity profile in the positive z direction is given by (Happel, 1959)

$$v_{zs}(\xi) = 2\langle v_{zs}\rangle\left[1-(\xi_c/\xi_e)^2\right] \times \frac{(\xi/\xi_e)^2-(\xi_c/\xi_e)^2+2\ln(\xi_c/\xi)}{3+(\xi_c/\xi_e)^4-4(\xi_c/\xi_e)^2+4\ln(\xi_c/\xi_e)}. \quad \text{(A13)}$$

It is possible to write two flux continuity equations at two different surfaces:

$$\xi = \xi_o, \qquad -D_{im}(\partial\phi_{im}/\partial\xi)_{\xi_o}\xi_o = (q_c/\delta_c)(\phi_{im}|_{\xi_o} - \phi^*_{im}|_{\xi_o})(r_c)_{\ln} \quad \text{(A14)}$$

$$\xi = \xi_c, \qquad -D_{il}(\partial\phi_{il}/\partial\xi)_{\xi_c}\xi_c = (q_c/\delta_c)(\phi_{im}|_{\xi_o} - \phi^*_{im}|_{\xi_c})(r_c)_{\ln}. \quad \text{(A15)}$$

Here ϕ^*_{im} is the hypothetical concentration of VOC in the porous membrane phase in equilibrium with the VOC concentration in the absorbent liquid phase:

$$\phi^*_{im}|_{\xi_c} = \phi_{il}|_{\xi_c}/H_{i2}. \quad \text{(A16)}$$

With the help of Eqs. A13, A14, A3, and A4, the following relations can be obtained:

$$(\partial\phi_{il}/\partial\xi)_{\xi_c} = Q(\phi_{im}|_{\xi_o} - H_{i1}\phi_{ig}|_{\xi=1}) \quad \text{(A17)}$$

$$H_{i1}P\phi_{ig}|_{\xi=1} - (a+P)\phi_{im}|_{\xi_o} + a\phi_{il}|_{\xi_c}/H_{i2} = 0 \quad \text{(A18)}$$

$$a = q_c(r_c)_{\ln}/\delta_c D_{ig} \quad \text{(A19)}$$

$$Q = [D_{im}/D_{il}]/\xi_c \ln\xi_o. \quad \text{(A20)}$$

Equation A17 is one of the boundary conditions required to solve Eq. A12. The other boundary conditions are

$$\xi = \xi_e, \qquad (\partial\phi_{il}/\partial\xi) = 0 \quad \text{(A21)}$$

$$-\xi_c\frac{L}{n}\left(D_{il}\frac{\partial\phi_{il}}{\partial\xi}|_{\xi_c}\right) = \int_{\xi_c}^{\xi_e}(\phi_{il}-\phi_{il,\text{in}})v_{zs}(\xi)r_i^2\xi\,d\xi. \quad \text{(A22)}$$

Substituting Eq. A13 into Eq. A12, the solution for shell-side concentration can be obtained with the help of boundary conditions A17, A21, and A22; it can be further rearranged at $\xi = \xi_c$ to

$$QH_{i1}Y\phi_{ig}|_{\xi=1} - QY\phi_{im}|_{\xi_o} - \phi_{il}|_{\xi_c} + \phi_{il,\text{in}} = 0 \quad \text{(A23)}$$

$$Y = y/(A\xi_e/\xi_c - B). \quad \text{(A24)}$$

The expressions for y, A, and B are given in Appendix B. Now the expressions for interfacial concentrations, $\phi_{im}|_{\xi_o}$ and $\phi_{ig}|_{\xi=1}$ provided in Eqs. 9 and 10, can be obtained by solving Eqs. A10, A18, and A23.

The bulk or cup-mixing gas-phase concentration at the inlet of the first segment of length Δz at $z = 0$, $\langle\phi_{ig}\rangle$, is obtained by simply equating the convective rate of transfer of i in the z direction with the diffusive rate of transfer of i in the radial direction at $\xi = 1$ (as in Eq. A9):

$$-(2/n)\pi LD_{ig}(\partial\phi_{ig}/\partial\xi)_{\xi=1} = \langle V_t\rangle(\langle\phi_{ig}\rangle - \phi_{ig,\text{out}}). \quad \text{(A25)}$$

Substituting the expressions of $(\partial\phi_{ig}/\partial\xi)|_{\xi=1}$ from Eq. A4 into Eq. A25, the expression for bulk gas-phase concentration, $\langle\phi_{ig}\rangle$, can be obtained as Eq. 7. The expression for the average liquid-phase concentration at the first segment outlet (Eq. 8) can be obtained in the way the average gas-phase concentration at the inlet of the segment was obtained.

Appendix B

$$y = \frac{\xi_c^4}{16\xi_e^2} + \frac{D\xi_c^2}{2} - \frac{\xi_c^2}{2}\ln\xi_c - A\xi_e\ln\xi_c + \frac{LD_{il}}{\kappa nr_i^2} - \frac{S}{e'} \quad \text{(B1)}$$

$$A = (3\xi_e/4) - (\xi_c^2/2\xi_e) + \xi_e\ln(\xi_c/\xi_e) \quad \text{(B2)}$$

$$B = (\xi_c/2) - (\xi_c^3/4\xi_e^2) \quad \text{(B3)}$$

$$D = 1 + \ln\xi_c - 0.5(\xi_c/\xi_e)^2 \quad \text{(B4)}$$

$$\kappa = \frac{2\langle v_{zs}\rangle\left[1-(r_c/r_e)^2\right]}{3+(r_c/r_e)^4-4(r_c/r_e)^2+4\ln(r_c/r_e)} \quad \text{(B5)}$$

$$S = a' + b' + c' + d' \quad \text{(B6)}$$

$$a' = \frac{\xi_e^8-\xi_c^8}{128\xi_e^4} + \left(\frac{\ln\xi_c}{48\xi_e^2} - \frac{\xi_c^2}{96\xi_e^4}\right)(\xi_e^6-\xi_c^6) - \frac{1}{48\xi_e^2}\left[\xi_e^6\left(\ln\xi_e - \frac{1}{6}\right) - \xi_c^6\left(\ln\xi_c - \frac{1}{6}\right)\right] \quad \text{(B7)}$$

$$b' = \frac{D}{4}\left(\frac{\xi_e^6 - \xi_c^6}{3\xi_e^2} + \left(\ln \xi_c - \frac{\xi_c^2}{2\xi_e^2}\right)(\xi_e^4 - \xi_c^4)\right) - \frac{D}{4}\left[\xi_e^4\left(\ln \xi_e - \frac{1}{4}\right) - \xi_c^4\left(\ln \xi_c - \frac{1}{4}\right)\right] \quad \text{(B8)}$$

$$c' = \frac{1}{12\xi_e^2}\left[\xi_c^6\left(\ln \xi_c - \frac{1}{6}\right) - \xi_e^6\left(\ln \xi_e - \frac{1}{6}\right)\right] + \left(\frac{\xi_c^2}{8\xi_e^2} - \frac{\ln \xi_c}{4} - \frac{1}{8}\right)\left[\xi_e^4\left(\ln \xi_e - \frac{1}{4}\right) - \xi_c^4\left(\ln \xi_c - \frac{1}{4}\right)\right] + (\ln \xi_e)^2 \xi_e^4/4 - (\ln \xi_c)^2 \xi_c^4/4 \quad \text{(B9)}$$

$$d' = -\frac{A}{4\xi_e}\left[\xi_e^4\left(\ln \xi_e - \frac{1}{4}\right) - \xi_c^4\left(\ln \xi_c - \frac{1}{4}\right)\right] + \left(\frac{A\xi_c^2}{2\xi_e} - A\xi_e \ln \xi_c - A\xi_e\right)\left[\xi_e^2\left(\ln \xi_e - \frac{1}{2}\right) - \xi_c^2\left(\ln \xi_c - \frac{1}{2}\right)\right] + A\xi_e\left[\xi_e^2(\ln \xi_e)^2 - \xi_c^2(\ln \xi_c)^2\right] \quad \text{(B10)}$$

$$e' = \frac{3}{4}\xi_e^2 + \frac{\xi_c^4}{4\xi_e^2} - \xi_c^2 + \xi_e^2 \ln\left(\frac{\xi_c}{\xi_e}\right). \quad \text{(B11)}$$

Manuscript received Jan. 22, 1996, and revision received Apr. 12, 1996.

Statement of Ownership, Management and Circulation required by 39 U.S.C. 3685 of September 30, 1996, for the *AIChE Journal*, Publication No. 002-580, issued monthly for an annual subscription price of $675.00 from 345 E. 47th St., New York, NY 10017, which is the location of its publication and business offices. The names and addresses of the Publications Director and Editors are: Managing Director, Publications, Stephen R. Smith, 345 E. 47th St., New York, NY 10017; Editor, Dr. Matthew V. Tirrell, Department of Chemical Engineering and Materials Science, University of Minnesota, Minneapolis, MN 55455; and Managing Editor, Haeja L. Han, 345 E. 47th St., New York, NY 10017. The owner is the American Institute of Chemical Engineers, 345 E. 47th St., New York, NY 10017. The known bondholders, mortgagees, and other security holders owning or holding 1% or more of the total amounts of bonds, mortgages, or other securities are: none. The purpose, function, and nonprofit status of this organization and the exempt status for federal income tax purposes have not changed during the preceeding 12 months. The following figures describe the nature and extent of *AIChE Journal* circulation. In each category the first number (*in italics*) is the *average number of copies of each issue during the preceding 12 months*. The number next to it, within parentheses (), is the actual number of copies of the single issue published nearest to the filing date. Total number of copies printed (net press run) *3,500* (3,500). Paid circulation: 1. sales through dealers and carriers, street vendors, and counter sales, none; 2. mail subscriptions, *2,578* (2,647). Total paid circulation *2,578* (2,647). Free distribution, by mail, carrier or other means, of samples, complementary, and other free copies: *45* (45). Total distribution: *2,758* (2,746). Copies not distributed: 1. office use, leftover, unaccounted, spoiled after printing, *877* (808). 2. returns from news agents, none. Total *3,500* (3,500). I certify that the statements made by me are correct and complete. Managing Director, Publications, Stephen R. Smith.